

## Fusion cross section of $\alpha$ -induced reactions for heavy target nuclei

Raj Kumar <sup>1,\*</sup>, Shilpa Rana <sup>1,†</sup>, M. Bhuyan <sup>2,‡</sup> and P. Mohr <sup>3,§</sup>

<sup>1</sup>*School of Physics and Materials Science, Thapar Institute of Engineering and Technology, Patiala 147004, India*

<sup>2</sup>*Center for Theoretical and Computational Physics, Department of Physics, Faculty of Science, University of Malaya, Kuala Lumpur 50603, Malaysia*

<sup>3</sup>*Institute of Nuclear Research (ATOMKI), H-4001 Debrecen, Hungary*



(Received 26 January 2022; accepted 11 March 2022; published 7 April 2022)

The fusion reactions induced by  $^4\text{He}$  projectiles on heavy target nuclei provide the reference to study the reaction dynamics of exotic halo nuclei. The present analysis aims to probe the effects of different nuclear density distributions and the effective nucleon-nucleon ( $NN$ ) interaction potentials on the fusion cross section of  $^4\text{He}$ -induced reactions for heavy target nuclei. The nuclear densities for the heavy nuclei are obtained within the well-known Skyrme-Hartree-Fock model and the relativistic mean-field (RMF) approach for the NL3\* parameter set. These densities are integrated with the density-dependent M3Y and the relativistic R3Y nucleon-nucleon ( $NN$ ) potentials to obtain the nuclear interaction potential. The fusion cross section and the astrophysical  $S$  factor are obtained for  $^4\text{He} + ^{208}\text{Pb}$ ,  $^4\text{He} + ^{209}\text{Bi}$ ,  $^4\text{He} + ^{235}\text{U}$ , and  $^4\text{He} + ^{238}\text{U}$  systems within the  $\ell$ -summed Wong model. The relativistic R3Y  $NN$  potential folded with RMF densities are observed to give a better fit to the available experimental data. Furthermore, a comparison is made for the results obtained using Hill-Wheeler and Wentzel-Kramers-Brillouin transmission coefficients for  $^4\text{He} + ^{208}\text{Pb}$  system. We found a reasonable fit in the cross section at around the Coulomb-barrier energies for both the approximations and also similar predictions can be drawn for all considered systems.

DOI: [10.1103/PhysRevC.105.044606](https://doi.org/10.1103/PhysRevC.105.044606)

### I. INTRODUCTION

The nuclear reactions between the light-mass projectiles and heavy targets are extremely important in extending the limits of the periodic table through the synthesis of new elements [1–4]. Moreover, the fusion reactions involving the radioactive beams serve as an optimal route to understand the correlation between the nuclear structure and the reaction dynamics [1–8]. Several light-mass nuclei with excessive neutrons or protons demonstrate halo structures occupying loosely bound nucleons. Various theoretical and experimental efforts have been devoted to studying the effects of breakup of these loosely bound light projectile nuclei on the fusion mechanism [1,4,7,8]. One of the examples of halo nuclei is  $^6\text{He}$ , which contains two loosely bound neutrons and is a so-called Borromean nucleus. As a result, the reactions induced by  $^6\text{He}$  halo nuclei on heavy targets such as the  $^6\text{He} + ^{208}\text{Pb}$ ,  $^6\text{He} + ^{209}\text{Bi}$ ,  $^6\text{He} + ^{235,238}\text{U}$ , etc., have been the interest of many studies [1,4,7,8]. The fusion dynamics of a stable and strongly bound  $^4\text{He}$  projectile with a heavy-mass target is a prerequisite to understand the effects of halo structure on the fusion process. In addition to this, the  $^4\text{He}$ -induced reactions also play a crucial role in various astrophysical

scenarios such as nucleosynthesis of stable neutron-deficient  $p$  nuclei which are bypassed by the dominating neutron capture processes [9–19]. The focus of the present analysis is the investigation of the fusion dynamics of  $^4\text{He}$ -induced reactions on heavy nuclei with  $Z \geq 82$ . The fusion mechanism of four reactions, namely,  $^4\text{He} + ^{208}\text{Pb}$ ,  $^4\text{He} + ^{209}\text{Bi}$ ,  $^4\text{He} + ^{235}\text{U}$ , and  $^4\text{He} + ^{238}\text{U}$ , is probed. The widely adopted double-folding approach [20] is used to obtain the nuclear potential between the interacting  $\alpha$  and heavy nuclei. One of the ingredients of the double-folding approach is the nuclear density distribution [20]. As a starting point, the density distributions for the considered heavy nuclei are taken from the well-established Skyrme-Hartree-Fock (SHF) formalism [21]. The SHF calculations ignore the relativistic effects, so we have also considered the nuclear densities arriving from the relativistic mean-field (RMF) formalism [22–31] with the NL3\* [28] parameter set. Both of the SHF and RMF approaches are successful in providing results compatible with the experimental observations for the nuclear bulk properties such as the binding energies, deformations, charge radii, and single-particle level ordering of the finite nuclei throughout the nuclear chart. Moreover, these approaches are also well developed for the description of nuclear matter characteristics. In the present analysis, we are interested in examining the effects of the nuclear densities of the heavy target nuclei arriving from the SHF and RMF calculations on the fusion dynamics of  $\alpha$ -induced reactions. The nuclear density distribution for the projectile ( $^4\text{He}$ ) was derived from the experimental data [32].

\*rajkumar@thapar.edu

†srana60\_phd19@thapar.edu

‡bunuphy@um.edu.my

§mohr@atomki.mta.hu

The second ingredient of the double-folding approach is the effective nucleon-nucleon ( $NN$ ) interaction [20]. The extensively used M3Y (Michigan 3 Yukawa) effective interaction with the inclusion of a realistic density dependence (called the DDM3Y potential) is adopted here. Moreover, the microscopic R3Y effective interaction derived from RMF equations [31,33–36] is also used here to account for the relativistic effects in the description of the fusion mechanism of  $\alpha$ -induced reactions. The  $\alpha$ -induced reaction cross sections are obtained within the  $\ell$ -summed Wong model given by Gupta and collaborators [37,38]. Because the main interest of the present analysis is the energy region of astrophysical relevance, the cross section is further represented in terms of the astrophysical  $S$  factor for all the reactions under study. The possible comparison of theoretical results is also made with the experimental data taken from the literature [39–41].

The study is organized as follows. The methodology used to obtain the fusion cross section in terms of nuclear density distributions and effective  $NN$  interaction is elaborated in Sec. II. The detailed discussion of calculations and results is carried out in Sec. III. Then the summary and conclusions of the present theoretical analysis are presented in Sec. IV.

## II. THEORETICAL FORMALISM

The key ingredient to probe the fusion mechanism of nuclear and astrophysical reactions is the total interaction potential formed between the fusing nuclei. This total potential includes the long-range charge-dependent Coulomb interactions, the angular-momentum-dependent centrifugal interactions, and the short-range nuclear interactions of an attractive nature. Thus, in the one-dimensional Schrödinger equation, the total potential as a function of the separation distance  $R$  between the two fusing nuclei can be written as

$$V_T^\ell(R) = V_n(R) + V_C(R) + V_\ell(R). \quad (1)$$

Here,  $V_C(R)$  denotes the Coulomb potential, i.e.,  $V_C(R) = Z_p Z_t e^2 / R$ , and  $V_\ell(R)$  denotes the centrifugal potential written as  $V_\ell(R) = \frac{\hbar^2 \ell(\ell+1)}{2\mu R^2}$ .  $V_n(R)$  is the nuclear potential, which is the most important ingredient of interaction potential and is calculated here within the well-known double-folding approach [20]:

$$V_n(\vec{R}) = \int \rho_p(\vec{r}_p) \rho_t(\vec{r}_t) V_{eff}(|\vec{r}_p - \vec{r}_t + \vec{R}| \equiv r) d^3 r_p d^3 r_t, \quad (2)$$

where  $\rho_p$  and  $\rho_t$  symbolize the density distributions for the interacting projectile and target nuclei, respectively. As discussed above, the nuclear densities for targets are obtained from the nonrelativistic SHF and the RMF approaches.  $V_{eff}$  is the effective  $NN$  interaction. Here, we have used two forms of effective interactions: the density-dependent Michigan 3 Yukawa (DDM3Y)  $NN$  potential and the relativistic R3Y  $NN$  potential.

The density of the  $\alpha$  projectile was derived from the experimental charge density distribution [32]. We used the data set in Ref. [32] with the largest range of momentum transfer which was provided by Sick [42]. The nucleon density was derived from the charge density distribution by unfolding the finite proton and neutron charge distributions using the

parameters given in Ref. [43]. The unfolding procedure leads to a root-mean-square (rms) radius of the  $\alpha$  projectile of 1.47 fm, which is about 12% lower than the charge radius of 1.68 fm [32,42]. This choice of the  $\alpha$  density has been used widely and has provided excellent results (e.g., Refs. [15,44,45]). For completeness it has to be noted that the influence of the unfolding procedure for the  $\alpha$  projectile on the potential in Eq. (2) is not as dramatic as one might expect from the 12% change of the rms radius of the  $\alpha$  projectile. The potential is composed of three ingredients ( $\rho_p$ ,  $\rho_t$ ,  $V_{eff}$ ), and thus the rms radius of the potential is affected only by about 1–2% by the unfolding procedure of the projectile density.

### A. Skyrme-Hartree-Fock approach for the nuclear densities

The self-consistent Hartree-Fock-Bogoliubov approach in combination with Skyrme forces is a well established and widely used model for the calculation of ground-state properties over the nuclear chart. In particular, nuclear proton and neutron densities are provided as part of the nuclear reaction code TALYS [46]. These SHF densities have been calculated by Goriely *et al.* and are based on detailed studies of mass formulas [21,47]. Because of their close similarity to experimental density distributions, these SHF densities have been adopted recently as the basis for the global Atomki-V2  $\alpha$ -nucleus potential [15]. Densities from a similar approach, but using a Gogny force instead of a Skyrme force, are also provided in TALYS. The differences between the SHF- and Gogny-based densities in the nuclear surface are tiny, leading to only marginal changes in the calculated fusion cross sections [48]. Thus, the Gogny-based densities are not included in the present study.

### B. Density-dependent M3Y effective $NN$ potential

The DDM3Y interaction has been used in many studies of  $\alpha$ - and heavy-ion-induced reactions (e.g., Refs. [20,49]) and  $\alpha$  decay [50,51]. The effective interaction  $V_{eff}$  factorizes into a radial dependence and a density dependence. The radial dependence is composed of a short-range repulsive part, a long-range attractive part, and a zero-range exchange part. The density-dependent part is calculated in the so-called “frozen density approximation.” The parameters of the density dependence are fitted to reproduce the strength of an effective  $G$ -matrix interaction [52,53]. Details on all parameters of the DDM3Y interaction are summarized in Ref. [44].

Double-folding  $\alpha$ -nucleus potentials with the DDM3Y interaction are often scaled by an overall normalization factor  $\lambda \approx 1.1$ –1.4, leading to volume integrals  $J_R$  of about 350 MeV fm<sup>3</sup> for heavy target nuclei [44,45]. Usually, the normalization factor is obtained by fits to the elastic scattering angular distributions. Such a normalization factor to the DDM3Y potentials is applied here in the combination with SHF densities only; this approach is based on the recently suggested Atomki-V2 potential [15,16] where the normalization parameter  $\lambda$  was chosen such that  $J_R = 342$  MeV fm<sup>3</sup> for magic and semimagic target nuclei and  $J_R = 371$  MeV fm<sup>3</sup> for nonmagic target nuclei. Contrarily, no normalization (i.e.,  $\lambda = 1.0$ ) was used for the RMF densities (see next section).

### C. Relativistic mean-field densities and R3Y $NN$ potential

In the RMF formalism, the atomic nucleus is considered as a system comprising protons and neutrons that are represented by Dirac spinors  $\psi$  of mass  $M$ . The interaction among these pointlike Dirac nucleons is assumed to take place through the exchange of effective pointlike particles: mesons and photons. The description of the many-body systems of nucleons and mesons is given by the phenomenological Lagrangian density of the form [22–31]

$$\begin{aligned} \mathcal{L} = & \bar{\psi} \{i\gamma^\mu \partial_\mu - M\} \psi + \frac{1}{2} \partial^\mu \sigma \partial_\mu \sigma \\ & - \frac{1}{2} m_\sigma^2 \sigma^2 - \frac{1}{3} g_2 \sigma^3 - \frac{1}{4} g_3 \sigma^4 - g_\sigma \bar{\psi} \psi \sigma \\ & - \frac{1}{4} \Omega^{\mu\nu} \Omega_{\mu\nu} + \frac{1}{2} m_\omega^2 \omega^\mu \omega_\mu - g_\omega \bar{\psi} \gamma^\mu \psi \omega_\mu \\ & - \frac{1}{4} \vec{B}^{\mu\nu} \cdot \vec{B}_{\mu\nu} + \frac{1}{2} m_\rho^2 \vec{\rho}^\mu \cdot \vec{\rho}_\mu - g_\rho \bar{\psi} \gamma^\mu \vec{\tau} \psi \cdot \vec{\rho}^\mu \\ & - \frac{1}{4} F^{\mu\nu} F_{\mu\nu} - e \bar{\psi} \gamma^\mu \frac{(1 - \tau_3)}{2} \psi A_\mu. \end{aligned} \quad (3)$$

Here  $g_\sigma$ ,  $g_\omega$ , and  $g_\rho$  symbolize the coupling constants for  $\sigma$ ,  $\omega$ , and  $\rho$  mesons having masses  $m_\sigma$ ,  $m_\omega$ , and  $m_\rho$ , respectively. The self-interaction properties of the nonlinear  $\sigma$ -meson field are taken into the account by the constants  $g_2$  and  $g_3$ . These parameters generate a long-range repulsive  $NN$  potential that plays a vital role in reproducing the saturation properties of nuclear matter.  $A_\mu$ ,  $\tau$ , and  $\tau_3$  represent the electromagnetic field, the isospin, and its third component, respectively.  $F^{\mu\nu}$ ,  $\Omega^{\mu\nu}$ , and  $\vec{B}^{\mu\nu}$  are the vector field tensors for the  $\omega^\mu$ ,  $\vec{\rho}_\mu$ , and photon, respectively, and are given as [28]

$$F^{\mu\nu} = \partial_\mu A_\nu - \partial_\nu A_\mu, \quad (4)$$

$$\Omega_{\mu\nu} = \partial_\mu \omega_\nu - \partial_\nu \omega_\mu, \quad (5)$$

and

$$\vec{B}^{\mu\nu} = \partial_\mu \vec{\rho}_\nu - \partial_\nu \vec{\rho}_\mu. \quad (6)$$

The equations of motion for nucleon and meson fields are obtained by solving the Euler-Lagrange equations under the mean-field approximation and are given as

$$\begin{aligned} (-i\alpha \cdot \nabla + \beta(M + g_\sigma \sigma) + g_\omega \omega + g_\rho \tau_3 \rho_3) \psi &= \epsilon \psi, \\ (-\nabla^2 + m_\sigma^2) \sigma(r) &= -g_\sigma \rho_s(r) - g_2 \sigma^2(r) - g_3 \sigma^3(r), \\ (-\nabla^2 + m_\omega^2) \omega(r) &= g_\omega \rho(r), \text{ and} \\ (-\nabla^2 + m_\rho^2) \rho(r) &= g_\rho \rho_3(r). \end{aligned} \quad (7)$$

The effective nucleon-nucleon interaction potential is derived from the field equations for mesons in the limit of one-meson exchange [31,33–36]. This so-called R3Y  $NN$  potential can be written in terms of meson masses and coupling constants

as [31,33–36]

$$\begin{aligned} V_{\text{eff}}^{\text{R3Y}}(r) = & \frac{g_\omega^2}{4\pi} \frac{e^{-m_\omega r}}{r} + \frac{g_\rho^2}{4\pi} \frac{e^{-m_\rho r}}{r} - \frac{g_\sigma^2}{4\pi} \frac{e^{-m_\sigma r}}{r} \\ & + \frac{g_2^2}{4\pi} r e^{-2m_\sigma r} + \frac{g_3^2}{4\pi} \frac{e^{-3m_\sigma r}}{r} + J_{00}(E) \delta(r). \end{aligned} \quad (8)$$

The term  $J_{00}(E) \delta(r)$  is a pseudopotential and takes care of the effects of single-nucleon exchange between the interacting nuclei. Here the R3Y  $NN$  interaction and relativistic densities for RMF are obtained for NL3\* [28] parameter sets. The nuclear density distributions coming from the SHF and RMF approaches are then integrated separately over the DDM3Y and relativistic R3Y  $NN$  potentials as per Eq. (2) to estimate the nuclear potential. A similar procedure is adopted in many of the recent studies from us and others and can be found in Refs. [31,33,34,36,54–56]. This nuclear potential is then employed to calculate the cross section and the astrophysical  $S$  factor by using the well-known  $\ell$ -summed Wong model described in the upcoming subsection.

### D. $\ell$ -summed Wong model

The  $\ell$ -summed Wong model is an extended version of the simplified Wong formula [37,38]. The  $\ell$ -summed Wong formula accounts for the actual angular momentum dependence of fusion barrier characteristics that was included in an approximate manner in the simplified Wong formula [37,38]. The fusion cross section in terms of the summation over the  $\ell$  partial waves is given by

$$\sigma(E_{\text{c.m.}}) = \frac{\pi}{k^2} \sum_{\ell=0}^{\ell_{\text{max}}} (2\ell + 1) P_\ell(E_{\text{c.m.}}). \quad (9)$$

Here,  $k = \sqrt{\frac{2\mu E_{\text{c.m.}}}{\hbar^2}}$  and  $E_{\text{c.m.}}$  denotes the energy of the colliding target-projectile system in the center-of-mass frame. The  $\ell_{\text{max}}$  values at above-barrier energies are determined using the sharp cutoff model [57] and are extrapolated for below-barrier energies. Its typical values for the considered reactions in the present work range up to  $18\hbar$ . The  $\mu$  denotes the reduced mass and  $P_\ell$  denotes the transmission coefficient for the total potential [see Eq. (1)] for the  $\ell$ th partial wave. Here, the penetrability  $P_\ell$  is obtained within the Hill-Wheeler (HW) approximation of the parabolic barrier [58] and can be written as

$$P_\ell^{\text{HW}} = \left[ 1 + \exp\left(\frac{2\pi(V_B^\ell - E_{\text{c.m.}})}{\hbar\omega_\ell}\right) \right]^{-1}. \quad (10)$$

The quantity  $\hbar\omega_\ell$  is called the barrier curvature and is evaluated at the barrier position  $R = R_B^\ell$  corresponding to the barrier height  $V_B^\ell$  as

$$\hbar\omega_\ell = \hbar \left[ \left. \frac{d^2 V_T^\ell(R)}{dR^2} \right|_{R=R_B^\ell} / \mu \right]^{\frac{1}{2}}. \quad (11)$$

The position ( $R_B^\ell$ ) and the height ( $V_B^\ell$ ) of the total interaction potential given in Eq. (1) are obtained from the following conditions:

$$\left. \frac{dV_T^\ell}{dR} \right|_{R=R_B^\ell} = 0, \quad (12)$$

$$\left. \frac{d^2V_T^\ell}{dR^2} \right|_{R=R_B^\ell} \leq 0. \quad (13)$$

The Hill-Wheeler approximation provides a simple expression [see Eq. (10)] for the transmission coefficient and has emerged to be quite successful in describing the fusion dynamics of various heavy-ion reactions [1,3,31,36–38]. However, at far-below-barrier center-of-mass energies, this parabolic approximation for the fusion barrier becomes inadequate and overestimates the fusion cross section [1,59]. This issue can be resolved by adopting the semiclassical Wentzel-Kramers-Brillouin (WKB) approximation [59–63] at deep sub-barrier energies. The transmission coefficient through the actual barrier within the WKB approximation can be written as

$$P_\ell^{\text{WKB}} = \exp \left\{ -\frac{2}{\hbar} \int_{r_1}^{r_2} \sqrt{2\mu[V_T^\ell(R) - E_{\text{c.m.}}]} \right\}. \quad (14)$$

Here,  $r_1$  and  $r_2$  are the classical turning points and are solutions of the equation on separation  $R$ ,

$$V_T^\ell(R) = E_{\text{c.m.}}. \quad (15)$$

*Astrophysical S factor.* The  $\ell$ -summed Wong model is successful in calculations of fusion and/or capture cross section at above and around the Coulomb-barrier energies. But the energies of astrophysical relevance lie far below the Coulomb barrier where the cross section diminishes due to the dominance of the Coulomb repulsion. So here the cross section is rescaled in terms of the astrophysical  $S$  factor [64] given by

$$S(E_{\text{c.m.}}) = E_{\text{c.m.}} \times \sigma(E_{\text{c.m.}}) \exp(2\pi\eta). \quad (16)$$

Here,  $\eta = \frac{Z_1 Z_2 e^2}{4\pi\hbar v}$  is the dimensionless Sommerfeld parameter and  $v = \sqrt{2E_{\text{c.m.}}/\mu}$  is the relative velocity of the target-projectile system.

### III. RESULTS AND DISCUSSION

The theoretical formalism elaborated in the previous section is now applied to study the fusion characteristics of four  $\alpha$ -induced reaction systems, namely, (a)  ${}^4\text{He} + {}^{208}\text{Pb}$ , (b)  ${}^4\text{He} + {}^{209}\text{Bi}$ , (c)  ${}^4\text{He} + {}^{235}\text{U}$ , and (d)  ${}^4\text{He} + {}^{238}\text{U}$ . The key input required to estimate the fusion probability of the two fusing nuclei is the nuclear interaction potential. Here, we have obtained the nuclear potential from the nuclear densities and the effective  $NN$  interaction within the double-folding approach. The nuclear density distributions of the interacting target nuclei are obtained from the nonrelativistic Skyrme-Hartree-Fock (SHF) approach and the relativistic mean-field (RMF) formalism for the NL3\* parameter set. Figure 1 shows the radial distributions of total densities (sum of proton and neutron densities) for all the four target nuclei considered in the present analysis. It can be noted from Fig. 1

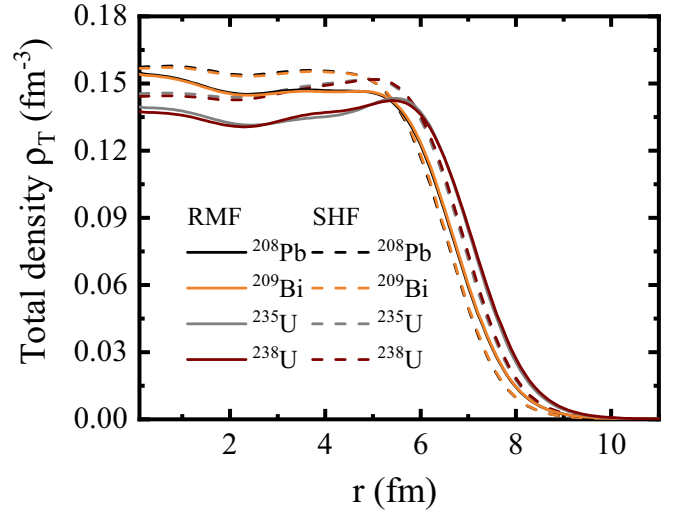


FIG. 1. Radial distributions of total density ( $\rho_T = \rho_P + \rho_N$ ) for all the target nuclei under study obtained from the RMF (solid lines) and the SHF (dashed lines) approaches. See text for details.

that the SHF densities are higher in the central region as compared to the RMF ones. This trend gets inverted in the nuclear surface region where the densities are observed to fall sharply. Moreover, the difference between the SHF and the RMF densities decreases as we move towards the surface region of the nuclei. The effect of this minute difference between SHF and RMF densities in the tail region on the interaction barrier characteristics and consequently on the fusion cross section is further investigated. For this, the target densities along with the experimental density of  ${}^4\text{He}$  [32] are integrated with the density-dependent M3Y and the relativistic R3Y nucleon-nucleon ( $NN$ ) interaction potentials. Thus, we get four sets of nuclear potentials for each reaction system denoted as M3Y-RMF, R3Y-RMF, M3Y-SHF, and R3Y-SHF. Here, M3Y-RMF signifies that the density-dependent M3Y  $NN$  potential is integrated over the nuclear density obtained from the RMF formalism to estimate the nuclear potential. Similar notations are used throughout the text from here onwards. The total interaction potential at  $\ell = 0$  (i.e., sum of nuclear and Coulomb potentials) as a function of separation distance is shown in Fig. 2 for the illustrative case of the  ${}^4\text{He} + {}^{238}\text{U}$  system. A significant difference between the total potential given by density-dependent M3Y and relativistic R3Y  $NN$  potentials is noticed at smaller separation distance ( $R$ ). The R3Y  $NN$  potential is observed to give a much deeper pocket as compared to the density-dependent M3Y  $NN$  potential. This shows that the R3Y potential given in terms of meson masses and coupling constants provides a much more attractive core of the  $NN$  potential. Further, it is also noted that the SHF density gives a deeper pocket as compared to the RMF density. As the separation between nuclei increases, the interaction potential is observed to become progressively repulsive which results in the formation of a fusion barrier. The magnified view of the barrier region of the interaction potential is given in the inset of Fig. 2. Moreover, the position ( $R_B$ ) and the height ( $V_B$ ) of the interaction barrier [see

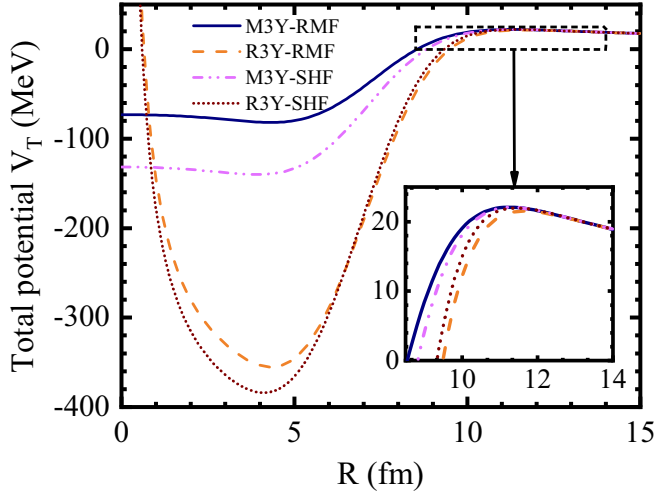


FIG. 2. The total potential ( $V_T$ ) at  $\ell = 0$  as a function of the separation distance ( $R$ ) for the  ${}^4\text{He} + {}^{238}\text{U}$  system calculated using the DDM3Y and the R3Y  $NN$  potentials along with the density distributions obtained from the SHF and the RMF approaches.

Eq. (1)] are also listed in Table I for all four reaction systems. It can be noted from Fig. 2 as well as from Table I that the R3Y-RMF and the M3Y-RMF nuclear potentials give the lowest and highest fusion barriers, respectively. This shows that the inclusion of relativistic effects in the description of the  $NN$  interaction potential lowers the fusion barrier, which consequently increases the fusion cross section. Moreover, the replacement of the RMF density for the target by that arriving from the SHF increases the barrier height when folded with the R3Y potential and lowers the barrier for the density-dependent M3Y  $NN$  potential. The fusion barrier height is observed to increase with the charge number of the target nuclei ( $Z_2$ ) due to the increase in the Coulomb repulsion. Also, a comparison of barrier heights for the  ${}^4\text{He} + {}^{235,238}\text{U}$  systems shows that the barrier height decreases as we move toward the neutron-rich (higher  $N/Z$  value) target. This indicates that the fusion probability increases with the target nucleus'  $N/Z$  ratio (isospin asymmetry).

As can be seen from Fig. 2, the M3Y-SHF potential is significantly deeper than the M3Y-RMF potential. This results from the scaling of the M3Y-SHF potential by the strength parameter  $\lambda = 1.38$ , whereas  $\lambda = 1.0$  was used for the M3Y-RMF potential (see Sec. II B). As a consequence of the deeper

potential, the effective barrier in the M3Y-SHF case is slightly lower than that for the M3Y-RMF case. If  $\lambda = 1.0$  were used also for the M3Y-SHF case, the effective barrier for the M3Y-SHF case would be slightly higher than that in the M3Y-RMF case. Next, we have calculated the fusion cross section for all the systems using the  $\ell$ -summed Wong model furnished with the SHF and the RMF formalisms. Both the SHF and the RMF approaches are well established to describe the structural properties of the finite nuclei throughout the nuclear chart and the saturation properties of the nuclear matter. The SHF approach is based on the idea of the energy functional, whereas the RMF formalism includes the mesonic degrees of freedom in the microscopic description of nucleon-nucleon interaction. Here we have studied the effects of nuclear density distributions obtained from both the SHF and RMF approaches on the fusion mechanism  $\alpha$ -induced reactions for the heavy target nuclei.

Moreover, the microscopic R3Y  $NN$  interaction potential derived from the RMF equations for mesons and the density-dependent M3Y  $NN$  potential are used in the double-folding approach in order to obtain the nuclear potential term of the interaction potential. It is worth mentioning here that the  $\ell$ -summed Wong model along with the RMF density distributions and the R3Y  $NN$  potential have been used successfully to study the fusion characteristics of various heavy and super-heavy nuclei [31,36,54]. Additionally this formalism has also been applied to probe the fusion cross section and the  $S$  factor of  ${}^{12}\text{C} + {}^{12}\text{C}$  at the center-of-mass energies of astrophysical significance [55]. Thus, it is interesting and crucial to explore the fusion dynamics of  $\alpha$ -induced reactions for heavy target nuclei at deep sub-barrier energies using the  $\ell$ -summed Wong model supplemented with the RMF and SHF nuclear density distributions.

The fusion cross section  $\sigma$  (mb) as a function of the center-of-mass energy  $E_{c.m.}$  (MeV) for (a)  ${}^4\text{He} + {}^{208}\text{Pb}$ , (b)  ${}^4\text{He} + {}^{209}\text{Bi}$ , (c)  ${}^4\text{He} + {}^{235}\text{U}$ , and (d)  ${}^4\text{He} + {}^{238}\text{U}$  systems is shown in Fig. 3. The experimental cross sections extracted from Refs. [39–41] are also given for comparison. The  $\ell$  values for these reaction systems are obtained from the sharp cutoff model [57] at above-barrier energies and are extrapolated for below-barrier energies. It is observed that the M3Y-RMF and the R3Y-RMF nuclear potentials give the lowest and the highest cross sections, respectively, at all center-of-mass energies. However, the difference in cross section decreases upon moving towards the energies above the Coulomb barrier. This is because the structure effects entering

TABLE I. The position  $R_B$  (in fm) and the height  $V_B$  (in MeV) of the fusion barrier obtained from the DDM3Y and the R3Y  $NN$  potentials along with the density distributions obtained from the SHF and the RMF approaches. See text for details.

System	M3Y-RMF		R3Y-RMF		M3Y-SHF		R3Y-SHF	
	$R_B$	$V_B$	$R_B$	$V_B$	$R_B$	$V_B$	$R_B$	$V_B$
${}^4\text{He} + {}^{208}\text{Pb}$	10.9	20.339 09	11.3	19.8211	10.9	20.338 17	11.1	20.150 72
${}^4\text{He} + {}^{209}\text{Bi}$	10.9	20.598 23	11.3	20.0752	10.9	20.587 82	11.1	20.398 73
${}^4\text{He} + {}^{235}\text{U}$	11.2	22.245 41	11.6	21.6868	11.3	22.149 05	11.4	22.046 55
${}^4\text{He} + {}^{238}\text{U}$	11.2	22.091 87	11.6	21.5284	11.3	22.073 22	11.4	21.9679

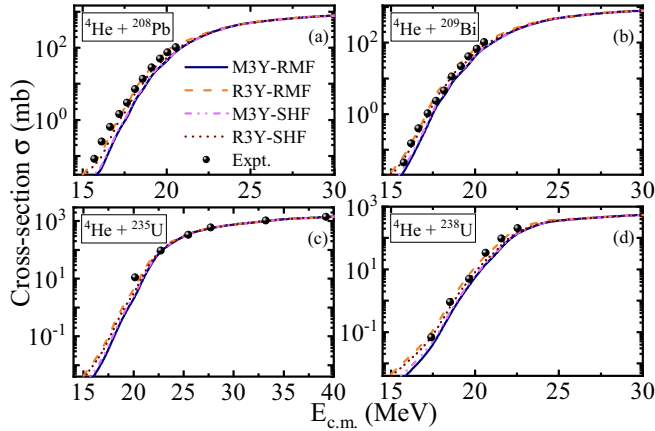


FIG. 3. The fusion cross section  $\sigma$  (mb) as a function of the center-of-mass energy  $E_{c.m.}$  (MeV) for (a)  ${}^4\text{He} + {}^{208}\text{Pb}$ , (b)  ${}^4\text{He} + {}^{209}\text{Bi}$ , (c)  ${}^4\text{He} + {}^{235}\text{U}$ , and (d)  ${}^4\text{He} + {}^{238}\text{U}$  systems calculated for the DDM3Y and the R3Y  $NN$  potentials along with the density distributions obtained from the SHF and the RMF approaches. The experimental data are taken from Refs. [39–41].

through the nuclear potential diminishes at the above-barrier energies and only the angular momentum effect persists [31]. The comparison of the theoretical cross section data with the experimental data shows that the relativistic R3Y effective  $NN$  interaction folded with the RMF densities gives comparatively better fit to the experimental data than the other combinations of density and  $NN$  potential.

As discussed in Sec. II, the magnitude of the cross section decreases as we move towards the far-below-barrier energy region of astrophysical significance. This can also be noticed from Fig. 3, where the cross section decreases by a factor of  $\approx 10^3$  as we move  $\approx 6$  MeV below the Coulomb barrier. The cause of this fall in cross section is the dominance of the Coulomb repulsion at energies far below the fusion barrier. To reduce the effects of the Coulomb repulsion, next we have plotted the cross section in terms of astrophysical  $S$  factor (MeV b) in Fig. 4 for all the considered systems. It can be noticed from Fig. 4 that the astrophysical  $S$  factor shows an increasing trend towards the lower center-of-mass energies. Again, the comparatively better fit to the experimental  $S$  factor is observed for the case of the R3Y-RMF nuclear potential. All these observations indicate that the inclusion of relativistic effects in the description of fusion characteristics enhances the cross section, especially at far-below-barrier energies of astrophysical relevance for all four  $\alpha$ -induced reactions considered in the present analysis. Recently, a possible appearance of a maximum in the  $S$  factor for the fusion of so-called light heavy ions between  ${}^{12}\text{C}$  and  ${}^{64}\text{Ni}$  at sub-Coulomb energies was discussed in Ref. [65]. Unfortunately, the experimental data of the systems under study are not conclusive for the case of  $\alpha$ -induced reactions.

*Hill-Wheeler vs WKB approximation.* The fusion cross sections and the  $S$  factors shown in Figs. 3 and 4 are calculated with the transmission coefficient obtained within the Hill-Wheeler approximation. This approximation is one of the parabolic fusion barriers that works well around and

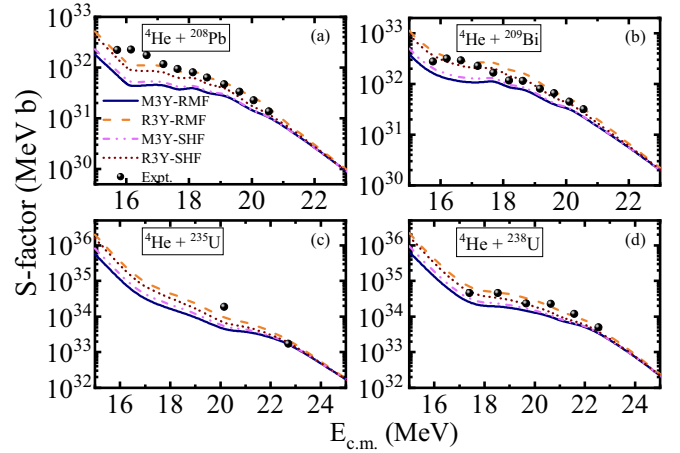


FIG. 4. The astrophysical  $S$  factor (MeV b) as a function of the center-of-mass energy  $E_{c.m.}$  (MeV) for the (a)  ${}^4\text{He} + {}^{208}\text{Pb}$ , (b)  ${}^4\text{He} + {}^{209}\text{Bi}$ , (c)  ${}^4\text{He} + {}^{235}\text{U}$ , and (d)  ${}^4\text{He} + {}^{238}\text{U}$  systems calculated for the DDM3Y and the R3Y  $NN$  potentials along with density distributions from the SHF and the RMF approaches. The experimental data are taken from Refs. [39–41].

above the Coulomb-barrier energies. However, at deep sub-barrier energies, the Hill-Wheeler approximation is observed to overestimate the fusion cross section, especially for reactions involving lighter nuclei [1,59]. To assess the validity of the Hill-Wheeler approximation at sub-barrier energies, we have also compared its result with the well-known WKB approximation [59–63], which gives the transmission coefficient through the exact fusion barrier. For this, we have only considered the nuclear potential obtained using the R3Y  $NN$  potential folded with the RMF density because, as evident from the above discussion, it gives better overlap with the experimental data than the other three sets of nuclear potentials. Figure 5(a) shows the comparison of the parabolic barrier (solid line) used in the Hill-Wheeler approximation with the actual fusion barrier (dashed line) obtained for the  ${}^4\text{He} + {}^{208}\text{Pb}$  system. It can be observed from Fig. 5(a) that the shape of the parabolic barrier is similar to that of the actual barrier at a smaller separation distance, whereas it differs at the larger separation. To explore its effects on the fusion mechanism, the cross section and the  $S$  factor as functions of the center-of-mass energy ( $E_{c.m.}$ ) are also shown in Figs. 5(b) and 5(c), respectively. It is observed that at energies well below the barrier, the WKB transmission coefficient gives a cross section and an  $S$  factor lower than those obtained within the Hill-Wheeler approximation. However, the cross sections and the  $S$  factors given by both approximations almost overlap at near-barrier energies. Further, the Hill-Wheeler approximation is observed to provide a reasonable fit to the experimental data at near-barrier energies for the  ${}^4\text{He} + {}^{208}\text{Pb}$  system. However, the inclusion of channel-coupling effects, which are not taken into account in the present analysis, may improve the comparison with the experimental data. A more systematic investigation of the effects of different transmission coefficients and channel couplings will be carried out in subsequent studies.

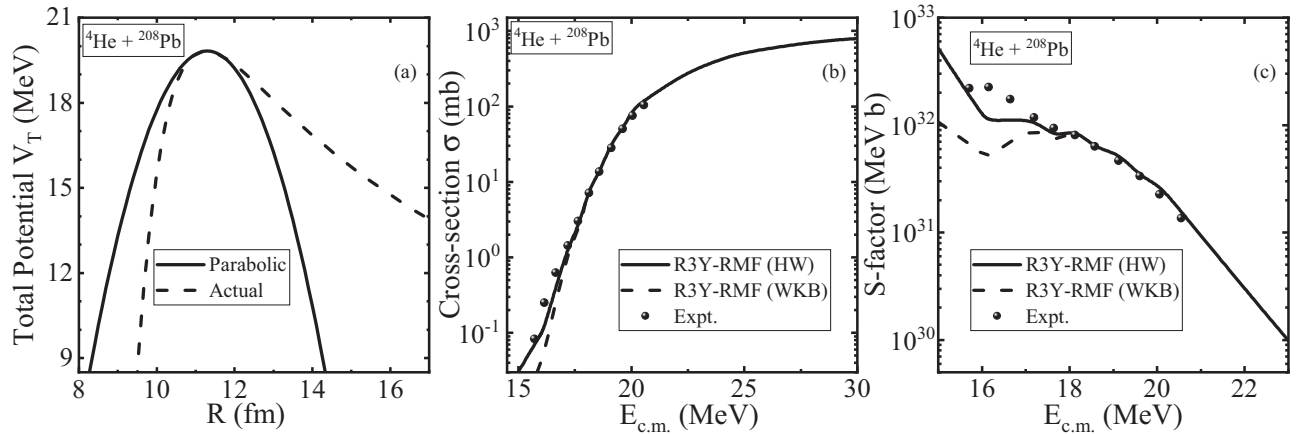


FIG. 5. (a) Comparison of the exact fusion barrier at  $\ell = 0\hbar$  (dashed line) obtained using the R3Y  $NN$  potential folded with the RMF density with pure parabolic barrier fit (solid line). (b) The fusion cross section and (c) the astrophysical  $S$  factor calculated using Hill-Wheeler (solid lines) and WKB (dashed lines) approximations for barrier transmission coefficients.

#### IV. SUMMARY AND CONCLUSIONS

The fusion characteristics of four  $\alpha$ -induced reactions for heavy target nuclei are explored within the well-known  $\ell$ -summed Wong model. The cross section is also rescaled in terms of the astrophysical  $S$  factor in order to minimize the effects of Coulomb repulsion at deep sub-barrier energies of astrophysical relevance. The effects of nuclear density distributions extracted from the nonrelativistic Skryme-Hartree-Fock (SHF) and the relativistic mean-field (RMF) formalisms for the NL3\* parameter set along with density-dependent M3Y and relativistic R3Y effective potentials are studied on the fusion mechanism of  $\alpha$ -induced reactions. It is observed that the relativistic R3Y  $NN$  potential integrated over the RMF nuclear density distributions gives the lowest barrier and consequently the highest fusion cross section for all the systems under study. The highest fusion barrier and the lowest cross section are observed for the density-dependent M3Y  $NN$  potential folded with the RMF densities. The comparison of theoretical calculations with the experimental cross sections shows that the R3Y-RMF nuclear potential gives comparatively better overlap than the other combinations.

Note that the R3Y-RMF approach can reproduce the experimental data without the adjustment of parameters. For a good reproduction of the experimental data, other potentials like the widely used M3Y-SHF potential [15,16] needed some read-

justment. Furthermore, to examine the relative dependence of the cross section and the  $S$  factor, the calculation is performed by using Hill-Wheeler and WKB transmission coefficients for the  ${}^4\text{He} + {}^{208}\text{Pb}$  system. We found a reasonable fit to the experimental data in the cross section at around the Coulomb-barrier energies for both the approximations and also similar predictions can be drawn for all considered systems. From the above observation, we can conclude that the inclusion of relativistic effects in the description of fusion dynamics enhances the cross section. Moreover, the fusion cross section for  $\alpha$ -induced reactions with heavy target nuclei at the sub-barrier energy region of astrophysical significance is more sensitive to the choice of nuclear potential as compared to the above-barrier energy region. A more comprehensive study involving more intermediate- and heavy-mass nuclei can be carried out to further probe the effects of different density distributions and effective  $NN$  interactions on the  $\alpha$ -induced reactions.

#### ACKNOWLEDGMENTS

One of the authors (S.R.) gratefully thanks Nishu Jain for useful discussions throughout the work. This work has been supported by the Science and Engineering Research Board (SERB) File No. CRG/2021/001229; FOSTECT Project No. FOSTECT.2019B.04; NKFIH (K134197); and FAPESP Project No. 2017/05660-0.

- [1] L. F. Canto, V. Guimaraes, J. Lubian, and M. S. Hussein, *Eur. Phys. J. A* **56**, 281 (2020).
- [2] M. Dasgupta, D. J. Hinde, N. Rowley, and A. M. Stefanini, *Annu. Rev. Nucl. Part. Sci.* **48**, 401 (1998).
- [3] *Nuclear Structure Physics*, edited by A. Shukla and S. K. Patra (CRC, Boca Raton, FL, 2020), Chap. 5.
- [4] B. B. Back, H. Esbensen, C. L. Jiang, and K. E. Rehm, *Rev. Mod. Phys.* **86**, 317 (2014).
- [5] A. Yoshida *et al.*, *Phys. Lett. B* **389**, 457 (1996).
- [6] M. Dasgupta, D. J. Hinde, K. Hagino, S. B. Moraes, P. R. S. Gomes, R. M. Anjos, R. D. Butt, A. C. Berriman, N. Carlin, C. R. Morton, J. O. Newton, and A. Szanto de Toledo, *Phys. Rev. C* **66**, 041602(R) (2002).
- [7] S. M. Lukyanov *et al.*, *Phys. Lett. B* **670**, 321 (2009).
- [8] L. F. Canto *et al.*, *Phys. Rep.* **424**, 1 (2006).
- [9] M. Arnould and S. Goriely, *Phys. Rep.* **384**, 1 (2003).
- [10] E. Somorjai, Z. Fülöp, Á. Z. Kiss, C. E. Rolfs, H. P. Trautvetter, U. Greife, and H. Oberhummer, *Astron. Astrophys.* **333**, 1112 (1998).
- [11] P. Scholz, H. Wilsenach, H. W. Becker, A. Blazhev, F. Heim, V. Foteinou, U. Giesen, C. Münker, D. Rogalla, P. Sprung, A. Zilges, and K. Zuber, *Phys. Rev. C* **102**, 045811 (2020).

- [12] S. Fujimoto, M. Hashimoto, K. Kotake, and S. Yamada, *Astrophys. J.* **656**, 382 (2007).
- [13] W. Rapp, J. Görres, M. Wiescher, H. Schatz, and F. Käppeler, *Astrophys. J.* **653**, 474 (2006).
- [14] C. Travaglio, F. K. Röpke, R. Gallino, and W. Hillebrandt, *Astrophys. J.* **739**, 93 (2011).
- [15] P. Mohr, Z. Fülöp, G. Gyürky, G. G. Kiss, and T. Szücs, *Phys. Rev. Lett.* **124**, 252701 (2020).
- [16] P. Mohr, Z. Fülöp, G. Gyürky, G. G. Kiss, T. Szücs, A. Arcones, and M. Jacobi, *At. Data Nucl. Data Tables* **142**, 101453 (2021).
- [17] A. Ornelas, P. Mohr, G. Gyürky, Z. Elekes, Z. Fülöp, Z. Halász, G. G. Kiss, E. Somorjai, T. Szücs, M.P. Takács, D. Galaviz, R. T. Güray, Z. Korkulu, N. Özkan, and C. Yalçın, *Phys. Rev. C* **94**, 055807 (2016).
- [18] T. Szücs, P. Mohr, G. Gyürky, Z. Halász, R. Huszánk, G. G. Kiss, T. N. Szegedi, Z. Török, and Z. Fülöp, *Phys. Rev. C* **100**, 065803 (2019).
- [19] L. Netterdon, P. Demetriou, J. Endres, U. Giesen, G. Kiss, A. Sauerwein, T. Szücs, K. Zell, and A. Zilges, *Nucl. Phys. A* **916**, 149 (2013).
- [20] G. R. Satchler and W. G. Love, *Phys. Rep.* **55**, 183 (1979).
- [21] S. Goriely, N. Chamel, and J. M. Pearson, *Phys. Rev. Lett.* **102**, 152503 (2009).
- [22] P. Ring, *Prog. Part. Nucl. Phys.* **37**, 193 (1996).
- [23] *Relativistic Density Functional For Nuclear Structure*, edited by J. Meng, International Review of Nuclear Physics Vol. 10 (World Scientific, Singapore, 2016).
- [24] J. Boguta and A. R. Bodmer, *Nucl. Phys. A* **292**, 413 (1977).
- [25] P.-G. Reinhard, *Rep. Prog. Phys.* **52**, 439 (1989).
- [26] B. D. Serot and J. D. Walecka, in *Advances in Nuclear Physics*, edited by J. W. Negele and E. Vogt (Plenum, New York, 1986), Vol. 16, p. 1.
- [27] Y. K. Gambhir, P. Ring, and A. Thimet, *Ann. Phys.* **198**, 132 (1990).
- [28] G. A. Lalazissis, S. Karatzikos, R. Fossion, D. Pena Arteaga, A. V. Afanasjev, and P. Ring, *Phys. Lett. B* **671**, 36 (2009).
- [29] D. Vretenar, A. V. Afanasjev, G. A. Lalazissis, and P. Ring, *Phys. Rep.* **409**, 101 (2005).
- [30] J. Meng, H. Toki, S. G. Zhou, S. Q. Zhang, W. H. Long, and L. S. Geng, *Prog. Part. Nucl. Phys.* **57**, 470 (2006).
- [31] M. Bhuyan and R. Kumar, *Phys. Rev. C* **98**, 054610 (2018).
- [32] H. De Vries, C. W. de Jager, and C. de Vries, *At. Data Nucl. Data Tables* **36**, 495 (1987).
- [33] B. B. Singh, M. Bhuyan, S. K. Patra, and R. K. Gupta, *J. Phys. G: Nucl. Part. Phys.* **39**, 025101 (2012).
- [34] B. B. Sahu, S. K. Singh, M. Bhuyan, S. K. Biswal, and S. K. Patra, *Phys. Rev. C* **89**, 034614 (2014).
- [35] C. Lahiri, S. K. Biswal, and S. K. Patra, *Int. J. Mod. Phys. E* **25**, 1650015 (2016).
- [36] M. Bhuyan, R. Kumar, S. Rana, D. Jain, S. K. Patra, and B. V. Carlson, *Phys. Rev. C* **101**, 044603 (2020).
- [37] R. Kumar, M. Bansal, S. K. Arun, and R. K. Gupta, *Phys. Rev. C* **80**, 034618 (2009).
- [38] C. Y. Wong, *Phys. Rev. Lett.* **31**, 766 (1973).
- [39] H. Freiesleben and J. R. Huizenga, *Nucl. Phys. A* **224**, 503 (1974).
- [40] R. Gunnink and J. W. Cobble, *Phys. Rev.* **115**, 1247 (1959).
- [41] J. L. Sida *et al.*, *Nucl. Phys. A* **685**, 51 (2001).
- [42] I. Sick, *Phys. Lett. B* **116**, 212 (1982).
- [43] F. Petrovich, R. J. Philpott, A. W. Carpenter, and J. A. Carr, *Nucl. Phys. A* **425**, 609 (1984).
- [44] P. Mohr, G. G. Kiss, Z. Fülöp, D. Galaviz, G. Gyürky, and E. Somorjai, *At. Data Nucl. Data Tables* **99**, 651 (2013).
- [45] U. Atzrott, P. Mohr, H. Abele, C. Hillenmayer, and G. Staudt, *Phys. Rev. C* **53**, 1336 (1996).
- [46] A. J. Koning, S. Hilaire, and M. C. Duijvestijn, *AIP Conf. Proc.* **769**, 1154 (2005).
- [47] N. Chamel, S. Goriely, and J. M. Pearson, *Nucl. Phys. A* **812**, 72 (2008).
- [48] G. G. Kiss, P. Mohr, G. Gyürky, T. Szücs, L. Csedreki, Z. Halász, Zs. Fülöp, and E. Somorjai (unpublished).
- [49] A. M. Kobos, B. A. Brown, R. Lindsay, and G. R. Satchler, *Nucl. Phys. A* **425**, 205 (1984).
- [50] P. Mohr, *Phys. Rev. C* **95**, 011302(R) (2017).
- [51] D. Deng and Z. Ren, *Phys. Rev. C* **96**, 064306 (2017).
- [52] J. P. Jeukenne, A. Lejeune, and C. Mahaux, *Phys. Rev. C* **16**, 80 (1977).
- [53] J. P. Jeukenne and C. Mahaux, *Z. Phys. A* **302**, 233 (1981).
- [54] S. Rana, R. Kumar, and M. Bhuyan, *Phys. Rev. C* **104**, 024619 (2021).
- [55] S. Rana, R. Kumar, and M. Bhuyan, *Astron. Nachr.* **342**, 473 (2021).
- [56] W. A. Yahya and B. D. C. Kimene Kaya, *Int. J. Mod. Phys. E* **31**, 2250002 (2022).
- [57] M. Beckerman, J. Ball, H. Enge, M. Salomaa, A. Sperduto, S. Gazes, A. DiRienzo, and J. D. Molitoris, *Phys. Rev. C* **23**, 1581 (1981).
- [58] D. L. Hill and J. A. Wheeler, *Phys. Rev.* **89**, 1102 (1953).
- [59] A. J. Toubiana, L. F. Canto, and M. S. Hussein, *Braz. J. Phys.* **47**, 321 (2017).
- [60] A. J. Toubiana, L. F. Canto, and M. S. Hussein, *Eur. Phys. J. A* **53**, 34 (2017).
- [61] K. Hagino and N. Takigawa, *Prog. Theor. Phys.* **128**, 1061 (2012).
- [62] Q. Haider, J. Y. Shapiro, and A. Sharma, *Nuovo Cimento A* **106**, 343 (1993).
- [63] D. J. Griffiths, *Introduction to Quantum Mechanics*, 2nd ed. (Pearson Prentice Hall, Hoboken, NJ, 2004), p. 327.
- [64] M. Beard, A. V. Afanasjev, L. C. Chamon, L. R. Gasques, M. Wiescher, and D. G. Yakovlev, *At. Data Nucl. Data Tables* **96**, 541 (2010).
- [65] V. V. Sargsyan, G. G. Adamian, N. V. Antonenko, and H. Lenske, *Phys. Lett. B* **824**, 136792 (2022).